In "Three-Dimensional Machine Vision", T. Kanade (ed)
Kluwer Academics Publisher, Boston, 1987, pp. 151-192

A Noncontact Optical Proximity Sensor for Measuring Surface Shape

Takeo Kanade and Michael Fuhrman

Computer Science Dept. and Robotics Institute
Carnegie-Mellon University
Pittsburgh, Pa. 15213

and

Equipment Development Division
Alcoa Laboratories
Alcoa Center, PA 15069

Abstract

We have developed a noncontact multi-light source optical proximity sensor that can measure the distance, orientation, and curvature of a surface. Beams of light are sequentially focused from light emitting diodes onto a target surface. An analog light sensor - a planar PIN diode - localizes the position of the resultant light spot in the field of view of the sensor. The 3-D locations of the light spots are then computed by triangulation. The distance, orientation, and curvature of the target surface is computed by fitting a surface to a set of data points on the surface.

The proximity sensor that has been built uses 18 light sources arranged in 5 conical rings. The sensor has a range of 10 cm where it can measure the distance of approximately 200 discrete points per second with a precision of 0.1mm, and then compute surface orientation with a precision of 1.0°. This sensor may be used by a robotic manipulator to home in on an object and to trace the object's surface.

1. Introduction

Noncontact proximity sensors that can measure the range and shape of a surface have useful robotic applications such as surface inspection, seam or edge tracking, obstacle avoidance, and homing a manipulator to an object. The simplest devices are optical switches that detect the presence of a

nearby surface [3], [11]. In these devices, a beam of light originating from a light source on the sensor illuminates a surface. The closer the surface is to the sensor the greater the intensity of the light reaching the sensor. By assembling the light emitter and the detector on small moving platforms the range of this device can be continuously altered [14]. However, this technique for measuring distance is sensitive to the orientation and reflectivity of a target surface as well as the distance of a surface. One method that was developed to overcome this limitation uses a single detector and several light sources. Distance is measured by comparing the relative intensities of the light reflected from a surface [13].

When light detectors sensitive to light spot position are used in a proximity sensor, distance can be measured by triangulation. The measurement then does not depend on the amount of reflected light reaching the sensor. Linear or planar CCD arrays [5], and linear or planar PIN diodes [1], [2], [6], [9], [8], [12] have been incorporated into proximity sensors. For example, in one application, a mirror deflects a beam of light into the field of view of a sensor. The position of the light spot is detected by a planar PIN diode and then correlated with the mirror position to compute distance and eventually the shape of a weld seam [2].

The proximity sensor that we have developed is configured around a planar PIN diode. Multiple conical arrays of light sources focus beams of light into the center of the field of view of the sensor where the distortion and nonlinearity of the sensor chip are smallest. The proximity sensor uses 18 light sources configured into 5 conical arrays. The sensor has a range of 10 cm where it can measure the distance of approximately 200 discrete points per second with a precision of 0.1 mm, and then compute surface orientation with a precision of 1°.

This paper focuses on the design and performance of the new proximity sensor. How well this type of sensor can measure the orientation of a target surface depends on the number of projected light spots, and how they are

distributed. Hence, the new sensor was designed with the aid of a statistical argument that takes into account the geometry of the sensor to minimize measurement uncertainty. The performance of the sensor was tested by measuring the distance and shape of various target surfaces.

2. Measurement of Distance and Shape

2.1. Overview

The proximity sensor is based on the principle of active illumination and triangulation. Figure 1 shows the basic configuration of the proximity The sensor head in this drawing consists of a ring of light sources, a lens, and a light spot position sensor chip.

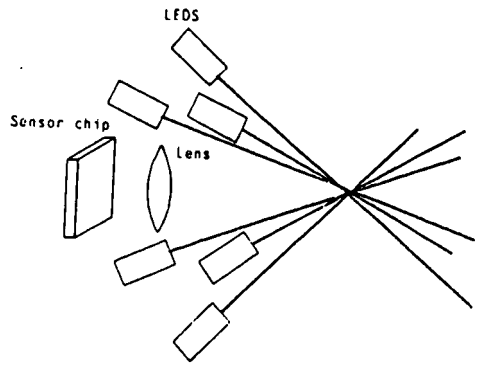

Figure 1: Configuration of the Multi-Light Source Proximity Sensor

The principle of operation is as follows. A beam of light emitted from the sensor head is interrupted by a target surface. The resultant light spot on the target surface is focused by the lens onto the analog light sensor that is sensitive to the intensity and position of a light spot in its field of view. Since the direction of the incident beam of light is known, and the light sensor measures the location of the light spot in the field of view, the three dimensional (3-D) coordinates of the light spot on the target surface can be computed by triangulation. The proximity sensor has multiple light sources, and as a result the coordinates of several discrete points on the surface can be measured. The average distance, orientation, and curvature of the target surface are computed by fitting a plane and then a quadric surface to this set of points.

Three features of the analog sensor chip make it an attractive device for use in the proximity sensor: its position linearity, its intrinsic ability to measure the centroid of a light spot on its surface, and its speed of response. The chip, a planar PIN diode, measures both the intensity and the position of the light spot on its surface. If the spot of light on a target surface is distorted because of the curvature or orientation of the surface, the sensor chip responds to the stimulus by measuring the coordinates of the centroid of the image of the light spot. To minimize error when computing the coordinates of the light spot, the spot size must be kept small. Therefore, light emitting diodes (LEDs) are used that have a light source diameter of about 150 μm.

2.2. Measuring the Distance of a Surface

The coordinates of a light spot on a target surface are computed by triangulation. The trajectory of each light beam that illuminates a surface is fixed and is measured in advance. The line of sight to the light spot on the target surface is obtained from the sensor chip. The calculation of the coordinates of the light spot is based on a simple optical model: first, the light source beam is a line, and thus the projected light spot is a point; second, the camera lens forms a flat, undistorted image; and finally the sensor chip is linear in finding the light spot position and is insensitive to defocus. Since the sensor is subject to small errors because of deviations from the simple model, they are treated as perturbations from the model and error corrections are calculated beforehand.

The position and orientation of a line in 3-D space can be defined by the

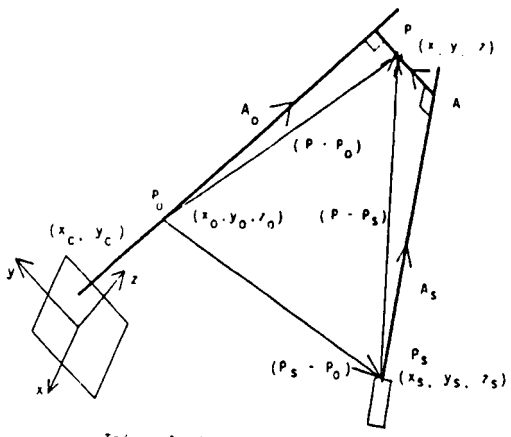

Triangulation:

P_o : Center of the camera lens
A_o : Vector defining the line of sight
P_s : Location of light source
A_s : Direction of light source
P : The chosen result of triangulation
A : A vector along the common normal

Figure 2: Calculation of Point Coordinates by Triangulation

coordinates of a point on the line and the direction cosines of the line. In Figure 2 light beam trajectory is defined by the light source origin $\mathbf{P}_s = (x_s, y_s, z_s)$ and the light beam direction vector $\mathbf{A}_s = (a_s, b_s, c_s)$. The line of sight has an orientation $\mathbf{A}_o = (a_o, b_o, c_o)$ that is defined by the camera lens center $\mathbf{P}_o = (x_o, y_o, z_o)$ and the centroid of the spot of light $\mathbf{P}_c = (x_c, y_c)$ on the sensor chip. Let us denote the coordinate of the spot position we want to locate as $\mathbf{P} = (x, y, z)$. In principle, the two three-dimensional lines (the light source beam and the line of sight) should intersect at the location of the spot on the surface. In practice, however, the two spatial lines thus obtained only come very close due to noise and the simplified optical model being used. We therefore determine the spot location $\mathbf{P}$ to be located along the line of closest approach (i.e., along the common normal) between the two skew lines. A set of equations from which the coordinates of the light spot can be calculated is found by observing that the four vectors consisting of the baseline from the center of the camera lens to the light source $(\mathbf{P}_s - \mathbf{P}_o)$, the light beam from the light source to the common normal $(A_s\mathbf{A}_s)$, the common normal $A\mathbf{A}$, and the line of sight from the common normal to the center of the camera lens $(-A_o\mathbf{A}_o)$ sum to zero, that is,

$$(\mathbf{P} - \mathbf{P}_o) + (A_s\mathbf{A}_s) + A\mathbf{A} \quad (-A_o\mathbf{A}_o) = 0. \tag{1}$$

Let the baseline have a length B and a direction specified by the unit vector $\mathbf{B} = (\mathbf{P}_s - \mathbf{P}_o)/|\mathbf{P}_s - \mathbf{P}_o|$. Then Equation (1) can be rewritten as

$$B\mathbf{B} + A_s\mathbf{A}_s + A\mathbf{A} - A_o\mathbf{A}_o = 0 \tag{2}$$

Taking the scalar product of Equation (2) first with the direction vector of the line of sight $\mathbf{A}_o$ and then with the direction vector of the light beam $\mathbf{A}_s$ leads to a set of two simultaneous equations. Noting that $\mathbf{A}_s \cdot \mathbf{A} = 0$ and $\mathbf{A}_o \cdot \mathbf{A} = 0$ yields

$$A_s\mathbf{A}_o \quad \mathbf{A}_s - A \quad = -B\mathbf{A}_o \quad \mathbf{B} \tag{3}$$

$$A_s - A_o\mathbf{A}_s \quad \mathbf{A}_o = -B\mathbf{A}_s \quad \mathbf{B} \tag{4}$$

After solving for A_s and A_o, the coordinates of the light spot can be chosen to be on the light beam or on the line of sight, or at any point along the common normal. Since the output of the sensor chip is subject to noise, and the position and orientation of each beam of light are stable quantities, we choose the computed coordinates of a light spot to lie on the light beam.

2.3. Surface Fitting

To estimate the position and orientation of a surface, a plane is fit to the set of three dimensional data points obtained by the proximity sensor. To estimate the curvature of a surface, a second order equation is fit. The accuracy of the calculation of position, orientation and curvature depends, therefore, on the accuracy of the individual data points, and the number and distribution of the data points on the surface. For example, if the points are too closely spaced, the orientation of the plane that is fit to the points will be very uncertain. These relationships were analyzed, and the results were used to design a sensor whose expected uncertainties are less than the design specifications.

Suppose there are n measured points on a surface, where each point (x_i, y_i, z_i) has an estimated total uncertainty in position of σ_i. A surface can be fit to this set of points using the method of least squares to determine the coefficients a_j in the equation

$$z(x,y) = \Sigma a_j X_j(x,y) \tag{5}$$

where $X_j(x,y)$ is a polynomial of the form $\Sigma c_{qr} x^q y^r$, as for example, when fitting a plane, $q + r \leq 1$, and when fitting a quadric surface, $q + r \leq 2$. We are concerned with how the uncertainty in the measured points and their distribution on the surface affects the uncertainty of the computed coefficients.

The values of the coefficients a_j are chosen so that they minimize the aggregate error E:

$$E = \sum_{i=1}^{n} \{\frac{1}{\sigma_i^2}(z_i - z(x_i,y_i))^2\} = \sum_{i=1}^{n} \{\frac{1}{\sigma_i^2}(z_i - \Sigma a_j X_j(x_i,y_i))^2\} \tag{6}$$

By minimizing E, each a_j can be computed by:

$$a_j = \sum_k \epsilon_{jk} \beta_k \tag{7}$$

where

$$[\epsilon_{jk}] = [\alpha_{jk}]^{-1} \tag{8}$$

$$\alpha_{jk} = \sum_{i=1}^{n} \{\frac{1}{\sigma_i^2} X_j(x_i,y_i) X_k(x_i,y_i)\} = \frac{1}{2} \frac{\partial^2 E}{\partial a_j \partial a_k} \tag{9}$$

$$\beta_k = \sum_{i=1}^{n} \{\frac{1}{\sigma_i^2} z_i X_k(x_i,y_i)\} \tag{10}$$

The symmetric matrix $[\alpha_{jk}]$ is known as the curvature matrix because of its relationship to the curvature of E in the coefficient space [4].

We can estimate the uncertainties of the coefficients, and determine their dependence on the geometry of the proximity sensor if we assume that fluctuations in the coordinates of the individual data points are uncorrelated, and assign the total uncertainty in the measurement of position to the variable z. The uncertainty of the coefficient a_j is then

$$\sigma_{a_j}^2 = \sum_{i=1} \sigma_i^2 \left(\frac{\partial a_j}{\partial z_i}\right)^2 \tag{11}$$

By calculating the partial derivatives of Equation (7), it follows that the uncertainties of the coefficients are proportional to the diagonal elements of the inverse of the curvature matrix [4], that is

$$\sigma_{a_j}^2 = \epsilon_{jj} \tag{12}$$

Let us first examine the case where the plane

$$z = Gx + Hy + I \tag{13}$$

is fit to a set of data points. Here we have set $a_1 = G$, $a_2 = H$, $a_3 = I$, $X_1 = x$, $X_2 = y$, and $X_3 = 1$ in Equation (5). The local surface normal is $\mathrm{N} = (G, H, -1)$. Since all of the measured points on a surface are at about the same distance from the sensor in any one measurement cycle, the total uncertainty σ_i can be taken as a constant σ for all of the data points. More accurately, since the uncertainty in the location of a light spot depends on where it is in the field of view and the intensity of the measured light, σ is considered an upper limit on the uncertainty in the location of a light spot. The curvature matrix for this case is

$$\alpha = \frac{1}{\sigma^2} \begin{vmatrix} \Sigma x_i^2 & \Sigma x_i y_i & \Sigma x_i \\ \Sigma x_i y_i & \Sigma y_i^2 & \Sigma y_i \\ \Sigma x_i & \Sigma y_i & n \end{vmatrix} \tag{14}$$

In many applications the proximity sensor will be used to maintain an orientation normal to a surface. The light sources can be arranged symmetrically so that the resulting spots of light on a flat surface facing the sensor perpendicularly satisfy the condition

$$\Sigma x_i = \Sigma y_i = \Sigma x_i y_i = 0 \tag{15}$$

that is, the α matrix is diagonal. The uncertainties in the coefficients of Equation (13) are then simply

$$\sigma_G = \frac{\sigma}{\sqrt{\Sigma x_i^2}} \tag{16}$$

$$\sigma_H = \frac{\sigma}{\sqrt{\Sigma y_i^2}} \tag{17}$$

$$\sigma_I = \frac{\sigma}{\sqrt{n}} \tag{18}$$

The angle between the optical axis of the proximity sensor and the surface normal is $\phi = \tan^{-1}\sqrt{G^2+H^2}$. The uncertainty in the angular orientation of a surface perpendicular to the sensor can be estimated by

$$\sigma_\phi^2 \leq \sigma_G^2 + \sigma_H^2 . \tag{19}$$

Equations (16) through (19) relate the uncertainty in the measured position and orientation of a surface with the number of data points, the uncertainty in their measurement, and their distribution on the surface.

2.4. Normal Curvature

To compute the curvature of a surface and to compute a more accurate value for the distance of a curved target surface from the proximity sensor, the second order equation

$$z = Ax^2 + Bxy + Cy^2 + Dx + Ey + F \tag{20}$$

of a surface is fit to the set of data points. The curvature of the target surface can be computed at any point from the coefficients of this equation. In particular, the normal curvature, κ_N, and the principal normal curvatures, κ_1 and κ_2, can be computed where the surface intersects the axis of the sensor.

Figure 3 shows the proximity sensor over a target surface. The projected

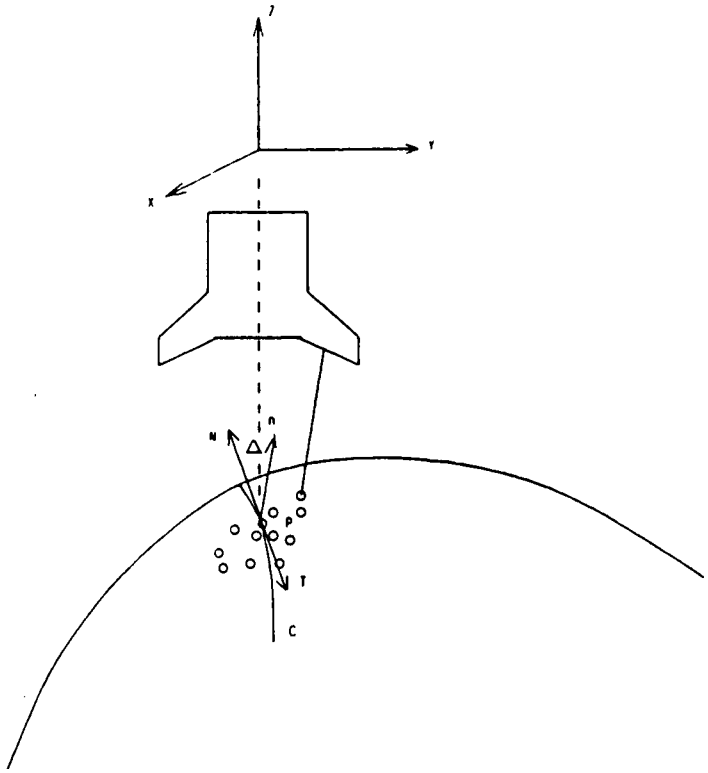

Figure 3: Measuring the Curvature of a Surface

light spots are shown as small circles on the surface. The intersection of the axis of the sensor with the target surface is located at P. The curve C on the surface is the intersection of the largest surface with a plane (not shown) containing the axis of the sensor. The vector n is the principal normal of the curve C at P; it lies in the intersecting plane. The vector T is tangent to the surface, and to the curve C at P. The vector N is normal to the surface at P. The angle between the vectors n and N is ϕ.

The equation of the fitted surface can be expressed as

$$\mathbf{R} = x\mathbf{i} + y\mathbf{j} + (Ax^2 + Bxy + Cy^2 + Dx + Ey + F)\mathbf{k}. \tag{21}$$

The surface normal, N, is given by

$$\mathbf{N} = \frac{\mathbf{R}_x \times \mathbf{R}_y}{|\mathbf{R}_x \times \mathbf{R}_y|} = \frac{((2Ax+By+D), -(Bx+2Cy+E), 1)}{\sqrt{(2Ax+By+D)^2 + (Bx+2Cy+E)^2 + 1}}, \tag{22}$$

where the subscripts x, y denote partial derivatives. The vector T, tangent to the surface, and to the curve C at P, is given by

$$\mathbf{T} = \frac{d\mathbf{R}}{ds}, \tag{23}$$

where $ds = |d\mathbf{R}|$. The curvature vector K, whose magnitude is the curvature of C at P is then given by

$$\mathbf{K} = \frac{d\mathbf{T}}{ds}. \tag{24}$$

The normal curvature vector, $\mathbf{K}_N$, is the projection of K onto the surface normal N. The component of $\mathbf{K}_N$ in the direction of N, κ_N, is called the normal curvature of C at P:

$$\mathbf{K}_N = (\mathbf{K}\cdot\mathbf{N})\mathbf{N} = \kappa_N \mathbf{N} \tag{25}$$

The magnitude of $\mathbf{K}_N$ is the curvature of a curve on the surface, in the plane of N, with tangent vector T at P.

To compute the curvature of a surface, one first computes the first and second fundamental coefficients of the surface [10]. The first fundamental coefficients of the surface are

$$\mathcal{E} = \mathrm{R}_x^{\,2} = 1 + (2Ax+By+D)^2 , \tag{26}$$

$$\mathcal{F} = \mathrm{R}_x \cdot \mathrm{R}_y = (2Ax+By+D)(Bx+2Cy+E) , \tag{27}$$

$$\mathcal{G} = \mathrm{R}_y^{\,2} = 1 + (Bx+2Cy+E)^2 \tag{28}$$

The second fundamental coefficients of the surface are

$$\mathcal{L} = \mathrm{R}_{xx} \cdot \mathrm{N} = 2A , \tag{29}$$

$$\mathcal{M} = \mathrm{R}_{xy} \cdot \mathrm{N} = B , \tag{30}$$

$$\mathcal{N} = \mathrm{R}_{yy} \cdot \mathrm{N} = 2C . \tag{31}$$

In terms of these coefficients, the normal curvature of the surface is given by

$$\kappa_N = \frac{\mathcal{L}dx^2+2\mathcal{M}dxdy+\mathcal{N}dy^2}{\mathcal{E}dx^2+2\mathcal{F}dxdy+\mathcal{G}dy^2} , \tag{32}$$

where the ratio $dx{:}dy$ specifies the direction of a line tangent to the surface at point P. In terms of the coefficients of the second order surface defined by Equation (20), the normal curvature at $x = y = 0$ is given by

$$\kappa_N = \frac{1}{\sqrt{1+E^2+D^2}} \; \frac{2[A\cos^2\theta+B\sin\theta\cos\theta+C\sin^2\theta]}{[(1+D^2)\cos^2\theta+2DE\sin\theta\cos\theta+(1+E^2)\sin^2\theta]} \tag{33}$$

Here, θ defines the orientation of the intersecting plane with respect to the $x-y$ axis.

The principal normal curvatures of the target surface where the axis of the sensor intersects the surface, κ_1 and κ_2, are the extreme values of Equation (32). In terms of the fundamental coefficients of the surface, κ_1 and κ_2 are the roots of the equation

$$(\mathcal{E}\mathcal{G}-\mathcal{F}^2)\kappa^2-(\mathcal{E}\mathcal{N}-2\mathcal{F}\mathcal{M}+\mathcal{G}\mathcal{L})\kappa+\mathcal{L}\mathcal{N}-\mathcal{M}^2 = 0 ,$$

The directions of the principal axes are given by the roots of the

$$(\mathcal{E}\mathcal{M}-\mathcal{F}\mathcal{L})\tan^2\theta+(\mathcal{E}\mathcal{N}-\mathcal{G}\mathcal{L})\tan\theta+\mathcal{F}\mathcal{N}-\mathcal{G}\mathcal{M} = 0$$

The principal curvature, κ_n, of the curve C at P is given by

$$\kappa_n = \frac{\kappa_N}{\cos\Delta} = \kappa_N \; \frac{\sqrt{1+D^2+E^2}}{\sqrt{1+D^2}} \tag{36}$$

where κ_N is computed in a direction tangent to C at P and Δ is the angle between N and n.

3. Measurement Error

The computed coordinates of a light spot in the field of view of the sensor is subject to error. The affects of various sources of error were taken into account in designing the sensor. Features of the sensor include: the beams of light from the sensor are focused into the center of the field of view where non-linearity and distortion are smallest; the light sources are modulated and the resultant signals from the sensor chip are synchronously detected; the resultant light spots on a target surface are small when compared to the area of the field of view of the sensor; and a means for adjusting the light source intensity has been provided so that the measured light intensity is within a small range.

One of the features of the sensor chip is it intrinsically measures the center of gravity of a light spot on its surface. If the shape of a target surface doesn't vary rapidly, the location of the light spot in the field of view of the sensor can be measured accurately. However, if the surface is

concave, light can be reflected about the surface. The center of gravity of the reflected light in the field of view will not coincide with the center of gravity of the projected light spot.

3.1. Distortion

To measure and then compensate for the distortion of the lens and the nonlinearity of the sensor, a square array of light spots was generated in the field of view of the sensor. The coordinates output by the sensor were then compared with the results computed according to the geometrical model of the sensor. A two dimensional transformation, $\{x_c, y_c\} \rightarrow \{x_c', y_c'\}$, maps the measured sensor chip coordinates into their expected values [7]. This transformation is applied to measured sensor chip coordinates each time a light source is turned on when the proximity sensor is in use.

3.2. Light Source Trajectories

The sensor chip was used to measure the trajectories of the beams of light that are emitted from the sensor head. To do this, a flat surface was mounted perpendicular to the optical axis of the sensor head. The z coordinate of a spot of light on the surface is simply the z position of the surface. As each light source was turned on, the sensor chip coordinates were measured and the x and y coordinates of each light spot were computed. By moving the plane along the z axis of the sensor, a set of points $\{x, y, z\}$ for each light source was acquired.

For each light source, a line was fit through a subset of the acquired data points, $\{x, y, z\}$, near the center of the field of view where spot size and nonlinearity are smallest. These lines were chosen to best estimate the light beam trajectories. The intersection of a line with the target plane yields the coordinates of a set of points $\{\bar{x}, \bar{y}, \bar{z}\}$. These points are considered to be the best estimate of point along the trajectory of a light beam.

3.3. Error Correction

Just as the set of points $\{\bar{x}, \bar{y}, \bar{z}\}$ were computed, now a set of points $\{x, y, z\}$ are computed for each LED by triangulation. The error is taken to be the difference between the coordinates $\{x, y, z\}$ computed by triangulation and the coordinates $\{\bar{x}, \bar{y}, \bar{z}\}$ computed according to the geometrical model.

Assuming that $(\bar{x}, \bar{y}, \bar{z})$ is the correct location of a light spot, let us set

$$\bar{x} = x + \epsilon_x , \tag{37}$$

$$\bar{y} = y + \epsilon_y , \tag{38}$$

$$\bar{z} = z + \epsilon_z . \tag{39}$$

It would be difficult to model the effect of the departures from the simplified model precisely to determine the terms ϵ_x, ϵ_y, and ϵ_z. However, since the errors are small and usually repeatable with respect to the measured spot position (x_c, y_c) on the sensor chip, we model them as a whole by means of polynomials, for example, by third order correction polynomials of the form

$$\begin{aligned} \epsilon_t = f_t(x_c, y_c) = {} & a_{t1}x_c^3 + a_{t2}x_c^2 y_c + a_{t3}x_c y_c^2 + a_{t4}y_c^3 \\ & + a_{t5}x_c^2 + a_{t6}x_c y_c + a_{t7}y_c^2 \\ & + a_{t8}x_c + a_{t9}y_c + a_{t10} \end{aligned} \tag{40}$$

where

$$t = x, y, z .$$

When the proximity sensor is calibrated, these polynomials are designed for each LED using a calibrated data set. During operation, the values

ϵ_x, ϵ_y, and ϵ_z computed by Equations (40) can be added to the spatial coordinates (x,y,z) computed by triangulation to obtain the corrected location of the spot.

4. Multiple Conical Arrays of Light Sources

Uncertainty in the measurement of surface orientation ultimately depends upon the uncertainty with which the sensor chip measures light spot position. Although the resolution of the sensor chip is potentially high (about 1/5000 across its surface), the precision of a single measurement is limited by several factors. The intensity of the light that reaches the sensor chip depends upon the distance, orientation and reflectivity of the target surface. The shape of a surface also affects the intensity distribution of the light spot on the sensor chip, causing a small error in measurement. However, because the sensor chip is very fast we can use redundant multiple light sources and choose the orientations and positions of the light sources so as to increase the accuracy of the sensor.

When measuring the distance of a surface, the region of greatest interest is generally the center of the field of view of the sensor. The effects of the various distortion and non-linearity are smallest near the optical axis. In addition, even if a spot of light is out of focus or grossly distorted by a surface, errors that are the result of a portion of the light spot falling beyond the edge of the sensor chip will be minimized. For these reasons the proximity sensor is configured using multiple conical arrays of light sources. In this way, several light sources are always focused near the optical axis over the range of the sensor.

Since the sensor chip measures the centroid of the intensity distribution on its surface, the distortion of the spot of light on a flat surface does not lead to an appreciable error. However, a large light spot size does decrease the linear range of the proximity sensor, and certainly will affect the measurement of curved surfaces. To minimize the size of the light spots, the

sensor uses light emitting diodes that were intended for fiber optic communication. These LEDs have a light source diameter of 150 microns. As a result the projected light spots on a target surface are on the order of 350 microns in diameter.

4.1. Placement and Orientation of Conical Arrays

Having decided that all of the light sources are to be arranged in multiple conical arrays, the angles of orientation for these light sources, and then the number of light sources comprising each cone, the number of cones, and the placement of the cones are determined by means of the statistical analysis of errors.

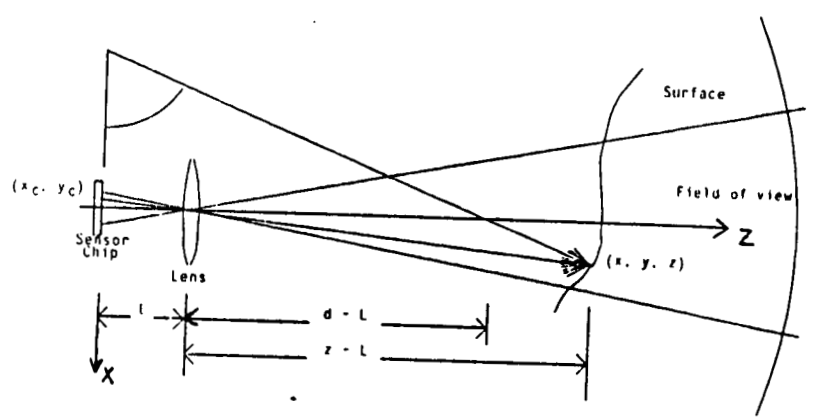

Figure 4: Camera Model of the Proximity Sensor

Figure 4 shows the locations of the sensor chip, the lens, and one light source focused on a point along the optical axis. The angle of the light beam relative to the x axis is θ. A line is drawn from the point on a surface intersecting the light beam, through the effective center of the lens, to the sensor chip. The equation of the beam of light in the x-z plane is

$$z = x \tan \theta + d \,. \qquad (41)$$

The x coordinate of the spot of light on the sensor chip is

$$x_c = \frac{L}{z-L} x \tag{42}$$

A small change in the z coordinate of the target surface by Δz corresponds to a shift in the spot of light on the sensor chip by Δx_c:

$$S = \frac{\Delta x_c}{\Delta z} = -\frac{L}{(z-L)\tan\theta} + \frac{L(z-d)}{(z-L)^2 \tan\theta}.$$

The larger the magnitude of S, the more sensitive the measurement. The orientation of the light beam θ can be chosen so any measurement of distance using a single light source will have a nominal sensitivity S_N in the center of the field of view, *i.e.*, at $z = d$. This condition places an upper bound on the value of θ:

$$\theta < \tan^{-1} \frac{L}{(d-L)} \frac{1}{S_N}. \tag{44}$$

Suppose one particular cone of light is generated using n light sources equally spaced in a circle. When a flat surface intersects the cone of light beams normal to the axis of the cone, the spots of light fall on a circle. The radius R of the circle is given by

$$R = |z-d| \cot\theta. \tag{45}$$

To determine the uncertainty in the orientation of a plane that is fit to these points, the mean-square values of the coordinates are first calculated. For $n \geq 3$:

$$\sum_{i=1}^{n} x_i^2 = R^2 \sum_{i=1}^{n} \cos^2 \frac{2\pi i}{n} = \frac{nR^2}{2}, \tag{46}$$

$$\sum_{i=1}^{n} y_i^2 = R^2 \sum_{i=1}^{n} \sin^2 \frac{2\pi i}{n} = \frac{nR^2}{2}. \tag{47}$$

Using Equations (16), (17), (18), and (19), the uncertainty in measured orientation when using a single cone of light can be calculated in terms of the uncertainty σ in the measurement of spot position, the radius of the circle of points, and the number of light sources:

$$\sigma_\phi \leq \frac{\sigma}{R} \frac{2}{\sqrt{n}}. \tag{48}$$

When using multiple cones of light, where the jth cone consists of n_j light sources focused towards a point d_j, the radius of the jth cone at z is

$$R_j = |z - d_j| \cot\theta_j. \tag{49}$$

The mean square value of the x coordinates of the data points is then

$$\sum_i x_i^2 = \frac{1}{2} \sum_j n_j \cot^2\theta_j (z-d_j)^2. \tag{50}$$

The uncertainty in measured orientation becomes

$$\sigma_\phi \leq \frac{2\sigma}{\sqrt{\Sigma n_j \cot^2\theta_j (z-d_j)^2}}. \tag{51}$$

This equation guides the determination of the number of light sources n_j in each cone, their orientation θ_j, and their placement d_j.

4.2. Design of the Proximity Sensor

Several guidelines guide the design of the proximity sensor. The sensor should be compact, with dimensions on the order of 10 cm, in order that it can be used by a robotic manipulator; the sensor should have a useful range of about 10 cm; the incident angle of the light beams on a target surface should be small to minimize light spot distortion; there should be at least three separate conical rings of light sources; and each individual light source should measure position with a sensitivity of at least 0.25 mm.

The primary constraint on the design of the proximity sensor was the light source intensity. The intensity of the light that is incident on a target surface depends on the intensity of the light emitter, the distance of the emitter from its focusing lens, and the diameter and focal length of the focusing lens. These last two quantities determine the size of the sensor and the number of light sources that can be mounted on the sensor head. The intensity of the reflected light that reaches the sensor chip depends on the distance of the camera lens from the target surface and the diameter of the lens.

In a tradeoff between sensitivity, range, and the size of the field of view, the distance from the camera lens to the plane that is in best focus was chosen to be 3.42 times the distance from the sensor chip to the lens. As a result, the area of the field of view that is in best focus is approximately 4.0 cm square. In the version of the sensor that has been built we use a 16mm, f/1.6 camera lens. If a camera lens with a shorter focal length were used, a smaller sensor could have been built. This sensor would focus over a closer range and have a wider field of view. However the sensitivity of the sensor would then be decreased at longer distances as the field of view of the sensor radially expanded. If we used a longer focal length camera lens the angular field of view would be smaller, and the sensitivity greater, but it is difficult to focus small spots of light with sufficient intensity at the greater distance that would then be in focus.

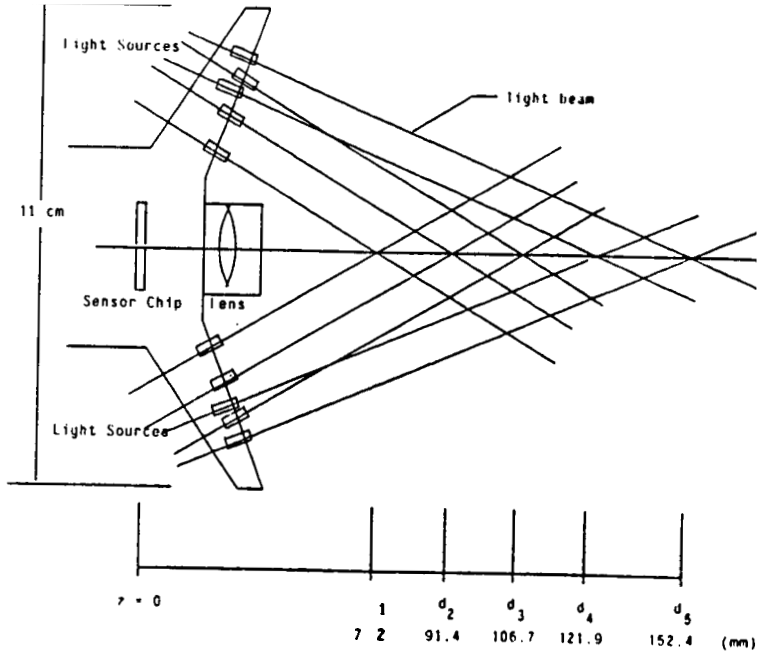

Figure 5: Geometry of the New Proximity Sensor

Figure 5 shows the configuration of the proximity sensor that has been built. To begin the analysis, we choose three cones of light each consisting of a three light sources. Equation (44) determined the choice of the angle of orientation of the light sources. With this angle chosen, we use Equation (51) to calculate the minimum spacing between the vertices d_1, d_2 and d_3 of the cones of light, where $z = d_2$ is in best focus.

First we have to estimate the uncertainty σ in the measurement of spot position at $z = d_2$. Referring to Equation (43) and Equation (44), we first set $\theta = 60°$, and $(d_2 - L) / L = 3.42$ and find $S_N = 6.67$. A smaller angle would increase the sensitivity of the sensor, but the light spot on a surface would then be further elongated. We assume that when a flat surface is measured, a signal to noise ratio can be achieved so that the effective resolution of the sensor chip is at least 1/500 its linear dimensions. This

corresponds to $\Delta x_c = 0.026$ mm , and a shift in the position of the target surface by $\Delta z = 0.15$ mm . This value of Δz is used to estimate σ_z. The total uncertainty σ is estimated by observing that when the position of a point is calculated by triangulation, the solution is constrained to lie on the line determined by the light beam. Since $\sigma^2 \approx \sigma_x^2 + \sigma_y^2 + \sigma_z^2$, and $\tan 60^o = \sqrt{3}$,

$$\sigma_z^2 \approx 3(\sigma_x^2 + \sigma_y^2) \tag{52}$$

and therefore,

$$\sigma^2 \approx 1.33\sigma_z^2. \tag{53}$$

The maximum value of the uncertainty in the measurement of surface orientation σ_ϕ occurs near the vertex of the middle cone. We use Equation (51) to calculate the minimum spacing between the vertices d_1, d_2 and d_3 of the cones of light by insisting the uncertainty in any single measurement of orientation at $z = d_2$ be less than 1.0^o (17.4 milliradians). Assuming these three cones are equally spaced, and consist of three light sources, we find

$$14.0 \text{ mm} \leq d_2 - d_1 = d_3 - d_2 \tag{54}$$

Figure 6 shows how the uncertainty in orientation σ_ϕ calculated by Equation (51) decreases as cones of light are added to the proximity sensor head. $\sigma_\phi(1)$ is graphed assuming a single cone of light consisting of three light sources is focused toward d_2. Then $\sigma_\phi(2)$ and $\sigma_\phi(3)$ are graphed as successive cones of light are added: first the cone with a vertex at d_3, then the cone with a vertex at d_1.

In order to further increase the accuracy of the sensor a second cone of light is focused at d_1 to augment the original light sources. In order to extend the range of the sensor, two more cones of light with an orientation of

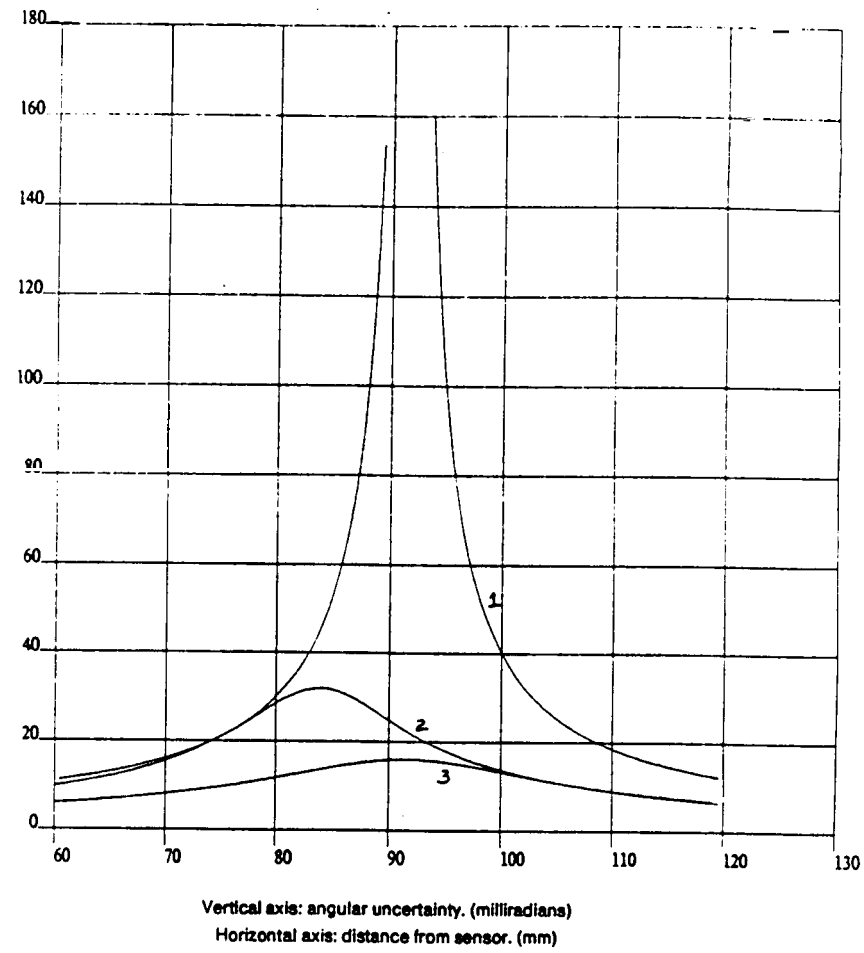

Figure 6: These graphs display the uncertainty when measuring the orientation of a flat target surface. Curves 1, 2, and 3 show the uncertainty when using a single, then two, and then three cones of light, each having three light sources

70° are focused towards points further along the optical axis. As a result, the range of the proximity sensor consists of two overlapping regions: first an inner region with a small field of view, a depth of 6 cm, and many redundant light sources where the sensor accurately measures the distance and shape of a surface, and then an outer region that extends the range of

the sensor by another 4 cm . The proximity sensor actually has an extended range of 20 cm. At this distance several of the light beams leave the field of view. However, the center of the field of view is devoid of light spots.

The computed distance and orientation of a target surface are estimated to be the values at the intersection of the surface with the axis of the sensor. If there are data points in this region, the estimate is more reliable than otherwise. The spacing of the vertices of the cones of light, and the orientations of the light sources determine how localized the data points are near the axis of the sensor over the range of the sensor. In the sensor that has been built, a light spot on the target surface is always within 5mm of the axis of the sensor.

The distances where the beams of light enter and leave the field of view of the sensor were computed for each light source. The angular field of view of the sensor depends on the active area of the sensor chip. Table 1 lists the entrance and exit distances for each light source assuming the active area of the sensor chip has a radius of 4 mm. In addition, the table lists the distances where each cone of light intersects the optical axis. From the table, one can see over what distances the cones of light overlap.

	Entrance (mm)	Axis Intercept (mm)	Exit (mm)
Cone 1	62.26	76.2	104.18
Cone 2	73.67	91.4	127.11
Cone 3	85.09	106.7	150.03
Cone 4	86.78	121.9	236.79
Cone 5	106.68	152.4	301.85

Table 1: Entrance and Exit Distances for Each Light Source.

This proximity sensor uses a total of 18 light sources arranged in 5 conical arrays. The diameter of the sensor is 11 cm. Assuming a sufficiently

high signal to noise ratio, the overall accuracy in the measurement of position when using the innermost 12 light sources is expected to be on the order of .1 mm. The accuracy in the measurement of surface orientation is expected to be better than 1°.

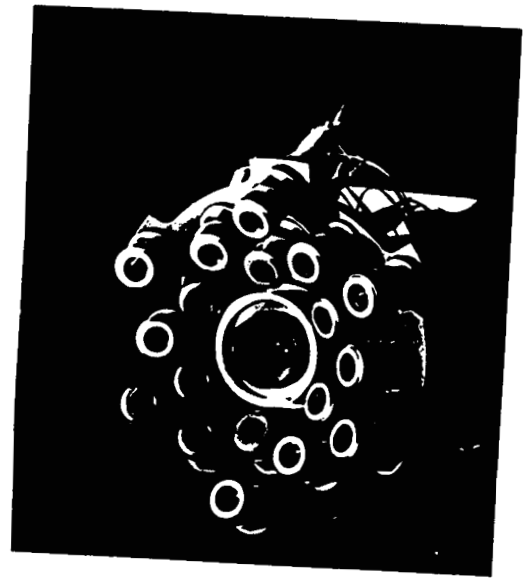

Figure 7: Photograph of the new proximity sensor

The proximity sensor head shown in Figure 7 is composed of a barrel that houses the analog sensor chip, and into which the camera lens and eighteen light sources are fixed. The barrel was machined from a single piece of aluminum to insure the concentricity of the cones of light sources with the optical axis of the camera lens and with the center of the sensor chip. Any

mitable C-mount lens can be mounted in front of the sensor chip. The light source is screwed into the flange of the barrel.

To summarize, the final parameters of the proximity sensor are:

Camera lens focal length: $f = 16$ mm
Sensor chip to lens distance: $L = 20.67$ mm
Distance from sensor chip to plane in best focus: $D = 91.4$ mm
Orientation of inner rings of light sources: $\theta_{1,2,3} = 60^\circ$
Orientation of outer rings light sources: $\theta_{4,5} = 70^\circ$
Number of light sources in ring 1: $n_1 = 6$
Number of light sources in outer four rings: $n_{2,3,4,5} = 3$
Distance between inner light source target points along the optical axis: 15.24 mm

This particular sensor head weighs approximately one pound. Future versions of the sensor can be constructed of composite materials to decrease the sensor's weight.

5. Performance

5.1. Measuring Distance and Orientation

The proximity sensor was used to measure the distance and orientation of flat target surfaces to determine the accuracy of the sensor. The test surfaces were moved by high resolution linear and rotary platforms in the field of view of the sensor. Each surface was rotated in 2° increments from −15° to +15°, and moved in 2 mm steps in front of the sensor. The distance and orientation of the surfaces were measured and compared with their expected values.

The results for a uniform white target surface are summarized in Figures 8 and 9. The graphs show the error in the measured distance and orientation of the surface as a function of the actual distance and orientation of the surface. The error in orientation is typically less than 2°, and the error in the measurement of distance is less than 0.2 mm.

The amplifier gains of the proximity sensor were set so that the sensor could measure the distance of a matte surface over a range of 10 cm. The

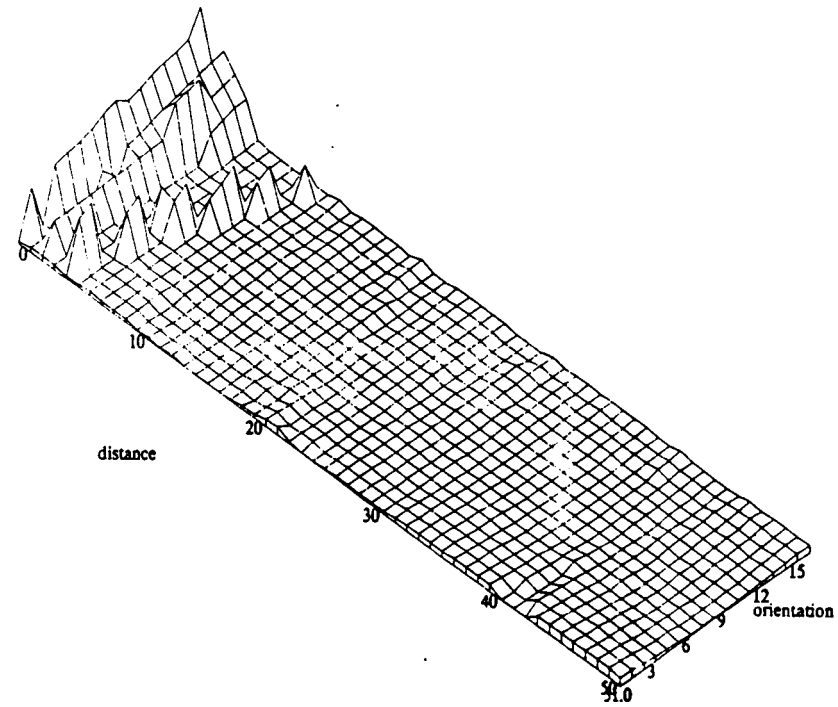

Figure 8: White surface: error in measured distance versus orientation and distance. The error in measured distance is typically less than 0.2mm

light intensity measured by the sensor agreed with the expected result when the white surface was used as a target. However, the reflectivity of an unpainted aluminum surface, for example, is less than that of a white surface, and in addition the reflected light has a large specular component. As a result, the range of the sensor was limited to 5 cm when measuring the distance of this type of surface. Either an insufficient amount of light is scattered by the surface towards the sensor, or alternatively, light is specularly reflected directly towards the sensor and overflows the amplifiers.

The measured coordinates of a light spot on a target surface also has a

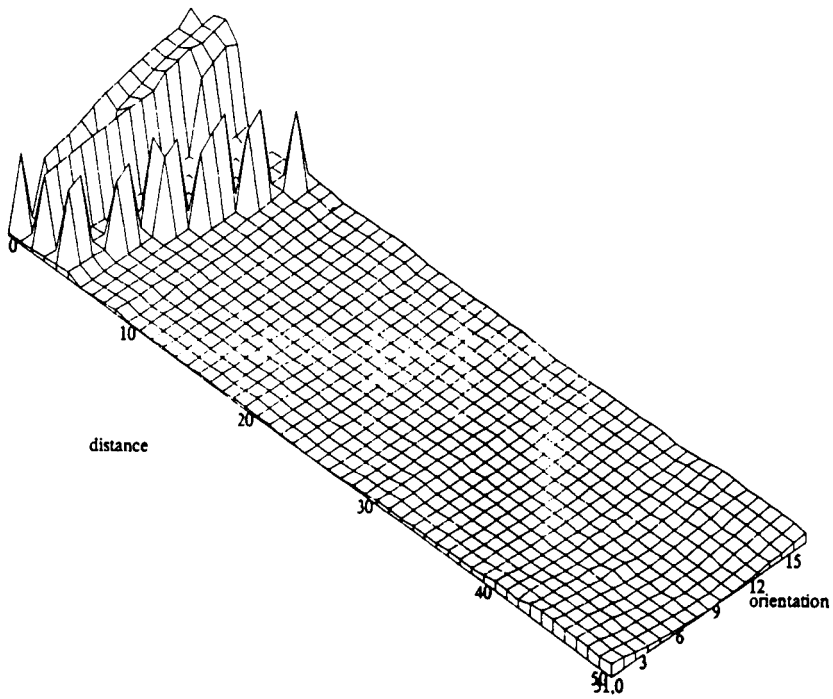

Orientation axis: -16° to 16° in 2° steps.
Distanc axis: 66.4 mm (0) to 166.4 mm (50) in 2 mm steps.

Figure 9: White surface: error in measured orientation versus orientation and distance. The error in measured orientation is typically less than 2°

small dependence on the intensity of the light reaching the sensor chip. As a result, when the sensor was calibrated for the white target surface and then used to measure the distance and orientation of the other target surfaces the results were in error. However, by recalibrating the proximity sensor for each of these surfaces, (that is, recomputing error correction polynomials), the performance of the sensor was improved so that the measurement error at normal incidence was less than 0.5 mm. Figures 10 through 13 show the errors computed for two target surfaces, a brushed and a tarnished aluminum surface, after recalibrating the sensor for each of these surfaces.

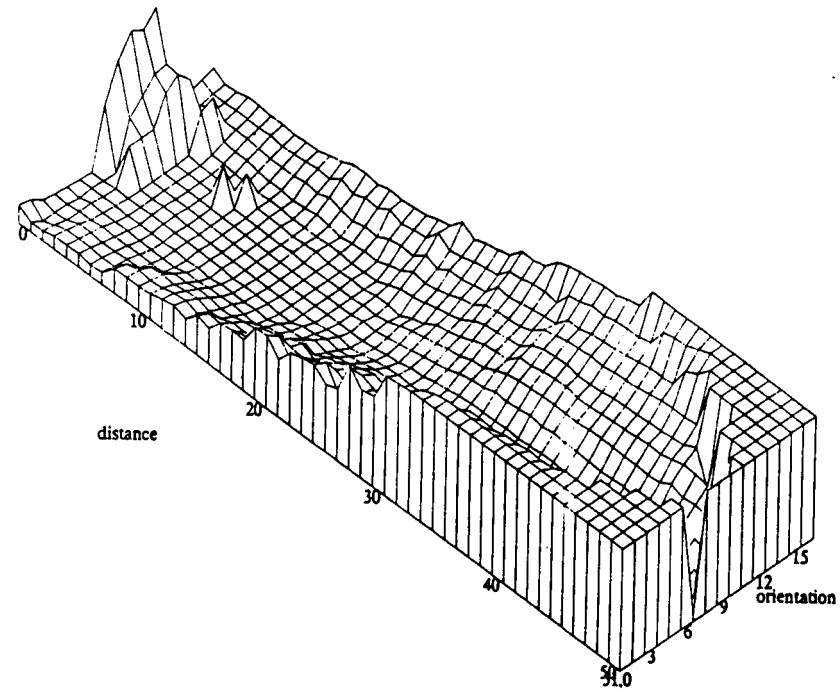

Orientation axis: -16° to 16° in 2° steps.
Distance axis: 66.4 mm (0) to 166.4 mm (50) in 2 mm steps.

Figure 10: Aluminum surface: error in measured distance versus orientation and distance after recalibrating the sensor.

5.2. Curvature

To measure the contour of a surface, a surface was moved through the field of view of the proximity sensor. At each position of the surface, the distance of the surface from the proximity sensor was measured, and the orientation and curvature of the surface were computed. The results were compared with the actual shape of each surface, and with shape of each surface that was computed assuming the proximity sensor behaved ideally.

The measurement of surface shape was simulated to evaluate the expected results. The coordinates of the resultant light spots on a simulated target surface were computed for each position of the surface. The distance,

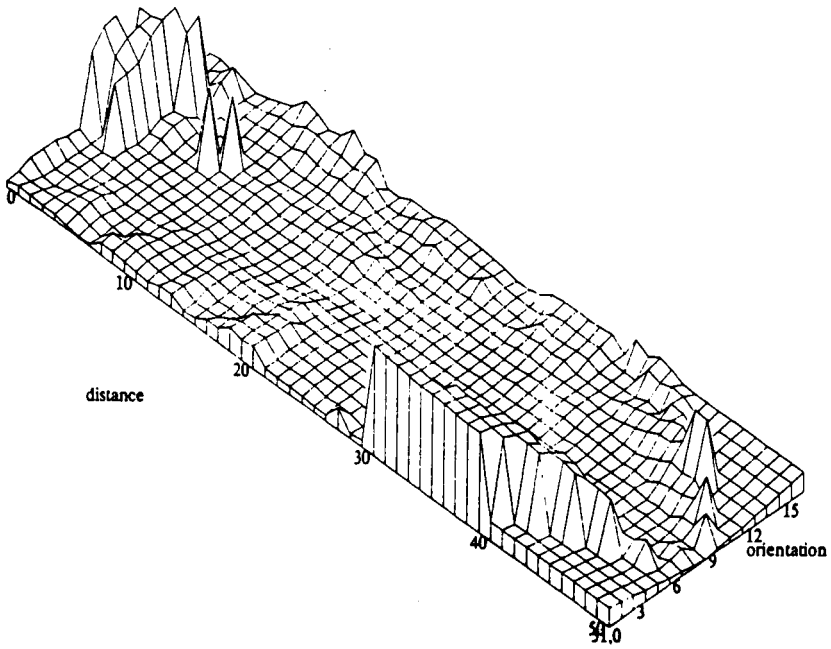

Figure 11: Aluminum surface: error in measured orientation versus orientation and distance after recalibrating the sensor.

orientation and curvature of the simulated target surface were computed, and the results were compared with the actual measurements.

Since measuring the contour of a surface uses only a small interval of the range of the sensor, relative measurement errors are generally small. For example, when a flat matte white with uniform reflectivity was moved across the field of view of the sensor, the error in measured distance was much less than the errors that were reported when the distance and orientation of the flat surface were varied over a range of 10 cm. In many applications of the proximity sensor, a target surface will be nearly flat. In addition, the sensor can be moved to maintain a fixed distance and orientation above a target

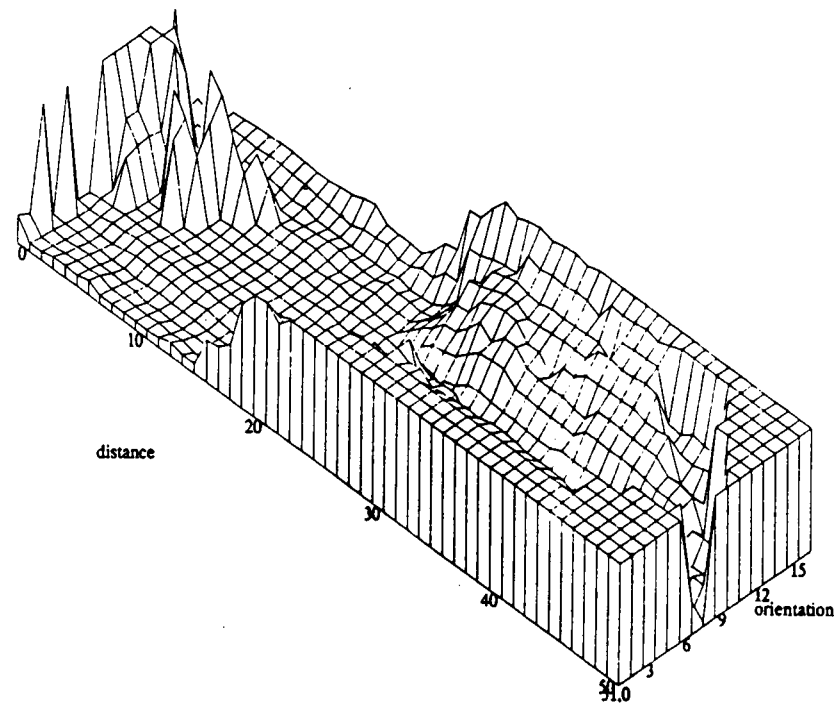

Figure 12: Tarnished surface: error in measured distance versus orientation and distance after recalibrating the sensor.

surface to achieve a better measurement.

The shapes of a cylinder and a cone were measured by moving each surface linearly across the field of view of the sensor a distance of 5 cm in 2 mm steps. The cylinder was in focus when closest to the sensor; the cone was positioned 6 mm further away. Both the cylinder and the cone were covered with a sheet of matte white paper. The cylinder had a 57.15 mm (2.25 inch) radius. In Figure 14 the contour of the cylinder is graphed as the sensor was moved across its surface.

The cone that was used as a target had a base angle of 81°. At the height at which the axis of the sensor intersected the surface of the cone, the cone

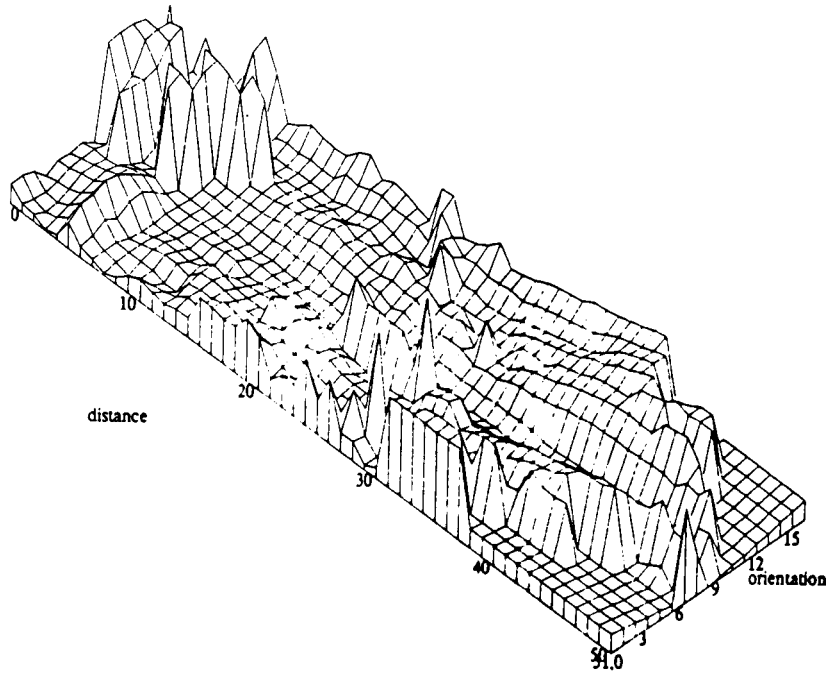

Orientation axis: -16° to 16° in 2° steps.
Distance axis: 66.4 mm (0) to 166.4 mm (50) in 2 mm steps.

Figure 13: Tarnished surface: error in measured orientation versus orientation and distance after recalibrating the sensor.

has a radius of 45 mm. The distance between the sensor and the cone was 97.4 mm at their closest position. This is 6 mm further away from the sensor than the distance of best focus. In Figure 15 the contour of the cone is graphed as the sensor was moved across its surface. Curve 1' shows the measurement results. Curve '2' shows the expected results that were computed according to the geometrical model of the sensor which assumes, for example, there were no extraneous reflections. Curve '3' shows the actual contour of the cone.

Figures 14 through 17 show that the proximity sensor can accurately measure the distance and orientation of a curved surface when the surface is

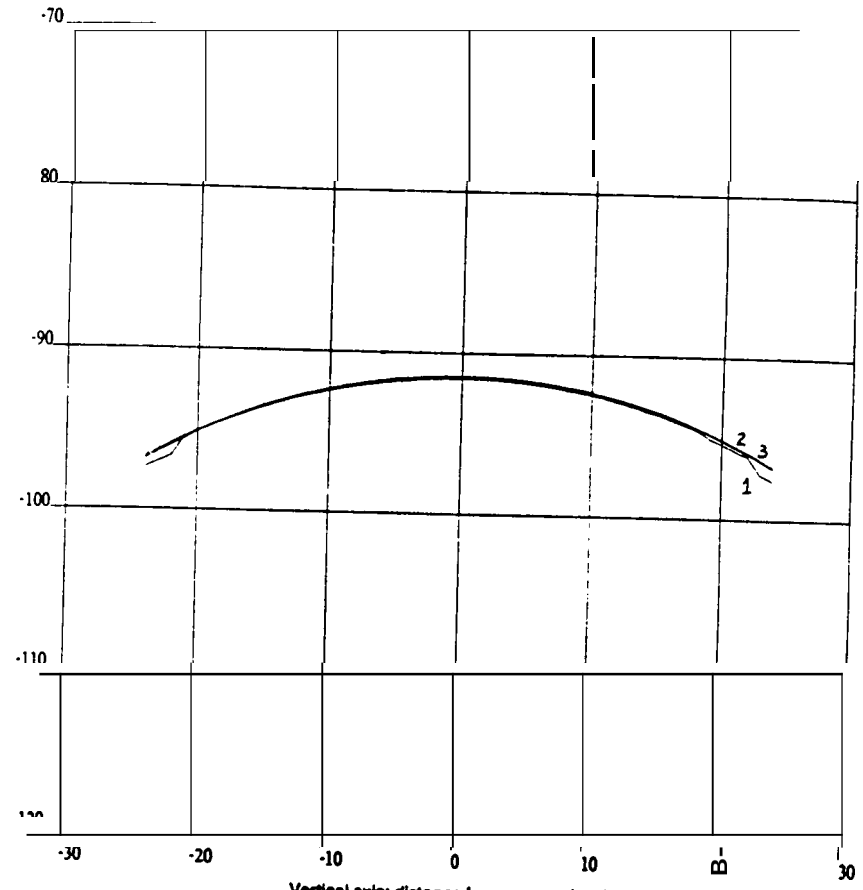

Vertical axis: distance from sensor. (mm)
Horizontal axis: motion of sensor across surface. (mm)

Figure 14: Contour of the surface of a cylinder: the measured 1 and the simulated 2 results, along with the actual 3 values

near normal to the axis of the sensor. When the orientation of each of these surfaces was computed from the coefficients of the second order equation, the results were not accurate. Fitting a quadric surface to the data points on a curved surface provides a better estimate of the range of a surface, but the gradient and the curvature of the surface are not stable. The local orientation of the target surfaces was better represented by fitting a plane to the data points. Figures 16 and 17 show the measurement results and the

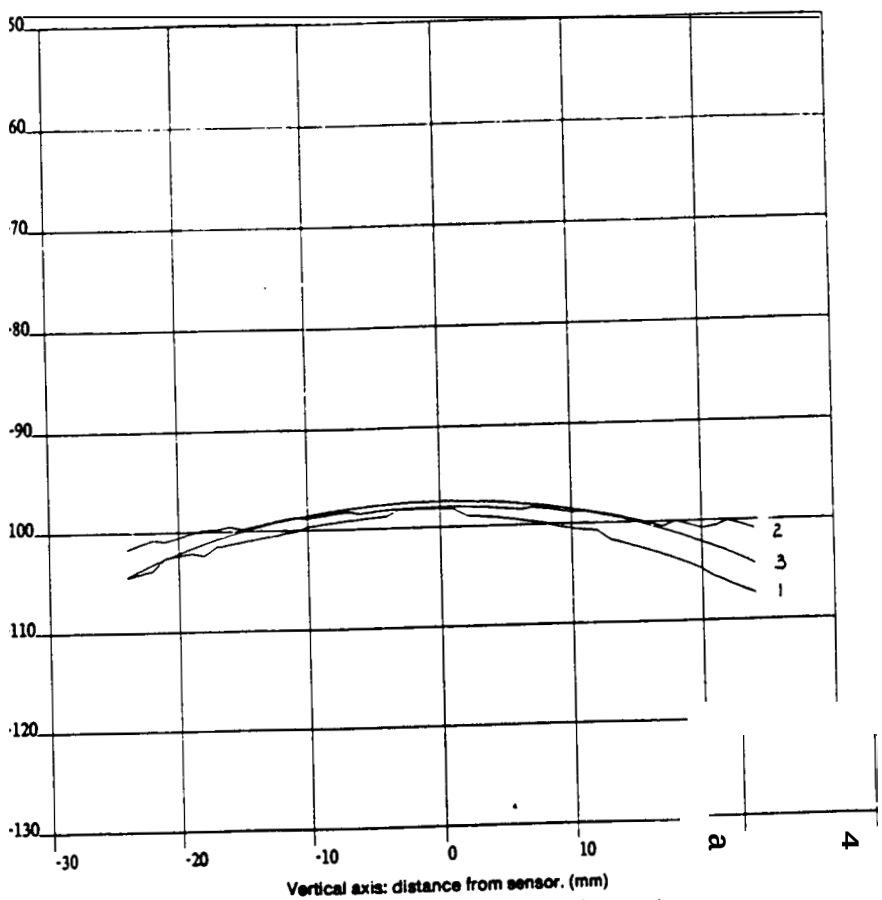

Figure 15: Contour of the surface of a cone: the measured 1 and the simulated 2 results, along with the actual 3 values

simulation results.

The principal normal curvatures, κ_1 and κ_2, of the cylinder and the cone were also computed. Figures 18 and 19 respectively show the smaller value for the computed principal radius of curvature of the cylinder and of the cone. The curves labeled '1' are the measured results and the curves labeled '2' show the simulation results. The solution for the curvature of the cylinder and the cone can be chosen where the other principal radius of

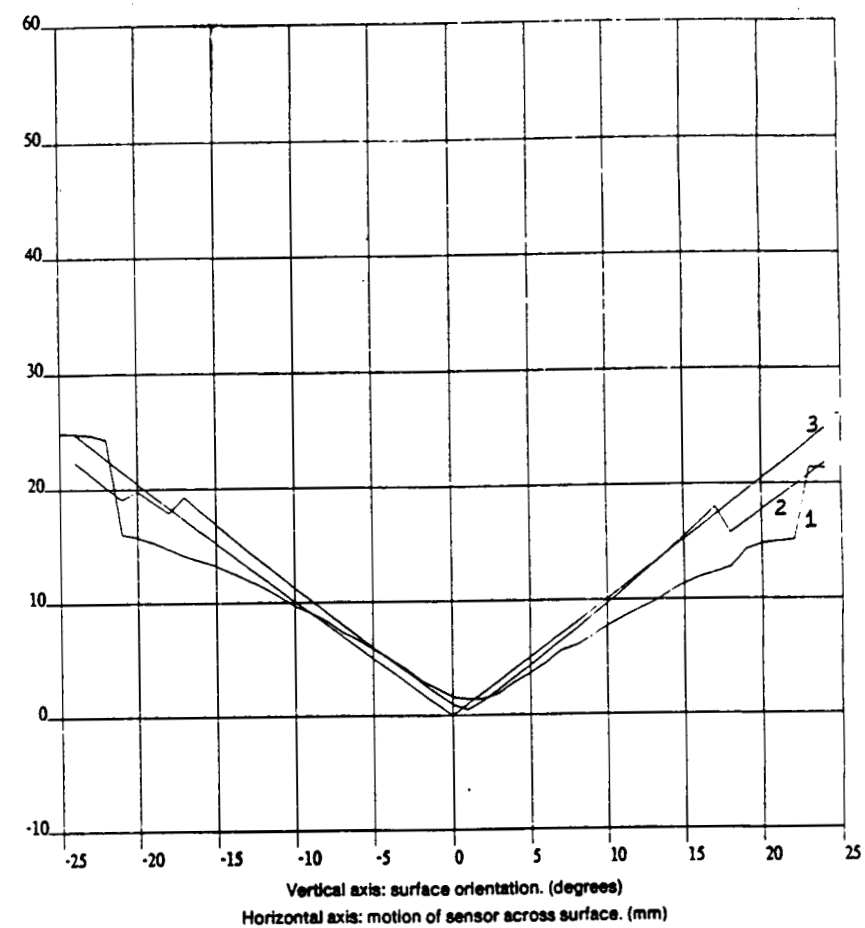

Figure 16: Surface orientation of the cylinder: measured 1 and simulated 2 results, and the actual value 3. The orientation is measured with respect to the axis of the proximity sensor

curvature has a maximum. For the cylinder this occurs where $x = -6$. For the cone this occurs where $x = 2$.

The proximity sensor can accurately measure the distance and orientation of a smooth surface when maintained at a near normal position relative to the surface. According to the simulation results, the proximity sensor has the potential to accurately measure the curvature of a surface.

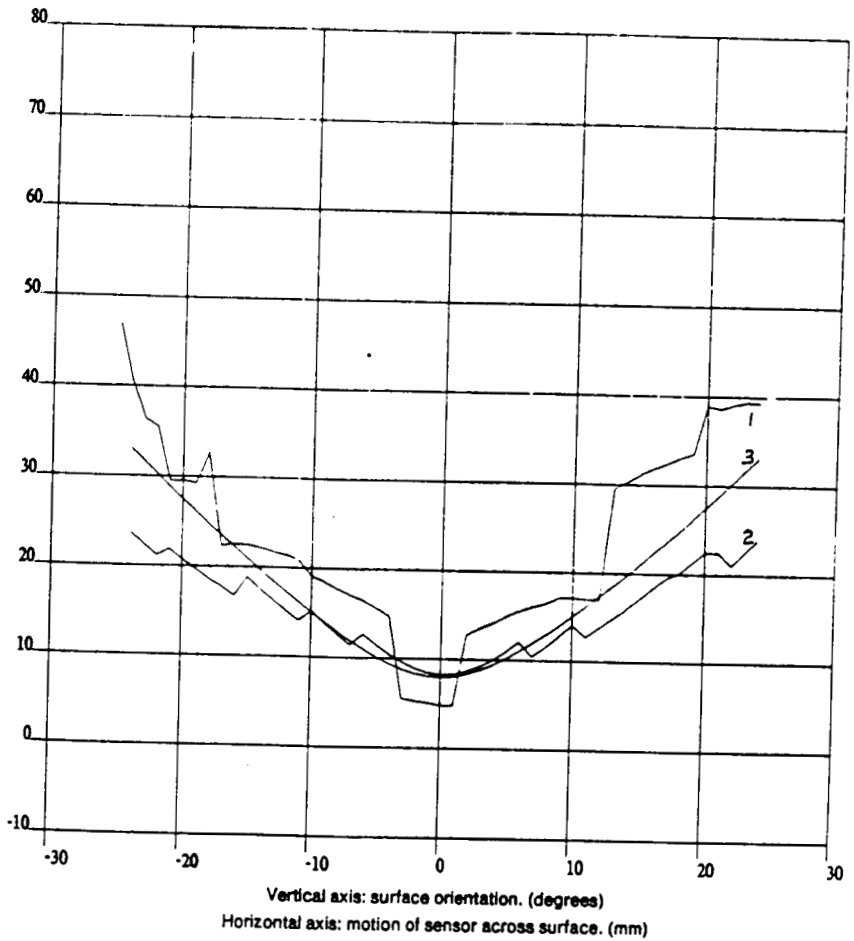

Figure 17: Surface orientation of the cone: measured 1 and simulated 2 results, and the actual value 3. The orientation is measured with respect to the axis of the proximity sensor

The simulated measurement of curvature is stable over a range of orientation and distance relative to a surface. However, the simulation did not take into account specular reflection of light toward the sensor head, finite light spot size and other perturbations. Either increasing the number of light sources, focusing smaller light spots onto the target surface, or using data points from earlier measurements in the computation, should increase

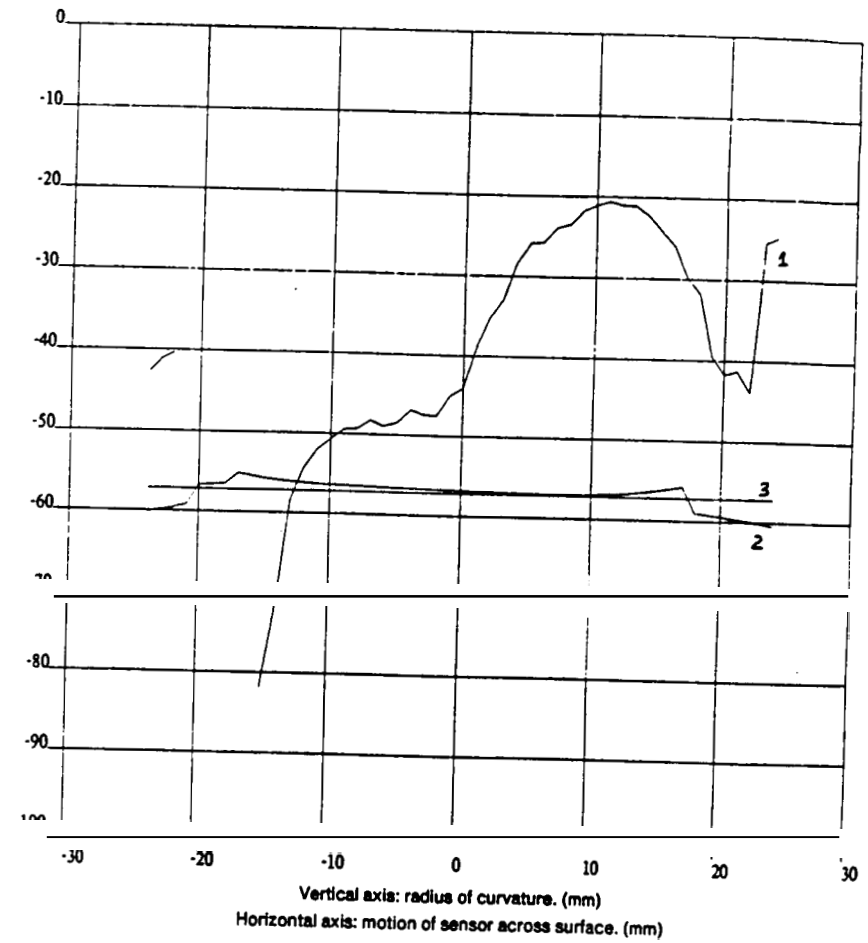

Figure 18: The smaller principal radius of curvature of a cylinder: measured 1 and simulated 2 results, and the actual value 3.

the accuracy of the computed curvature.

6. Conclusion

A new compact multi-light source proximity sensor has been developed. The sensor is based on the principle of active illumination and triangulation: each time a light source is pulsed, the coordinates of the resulting spot of the light on a surface are calculated. The proximity sensor that has been built

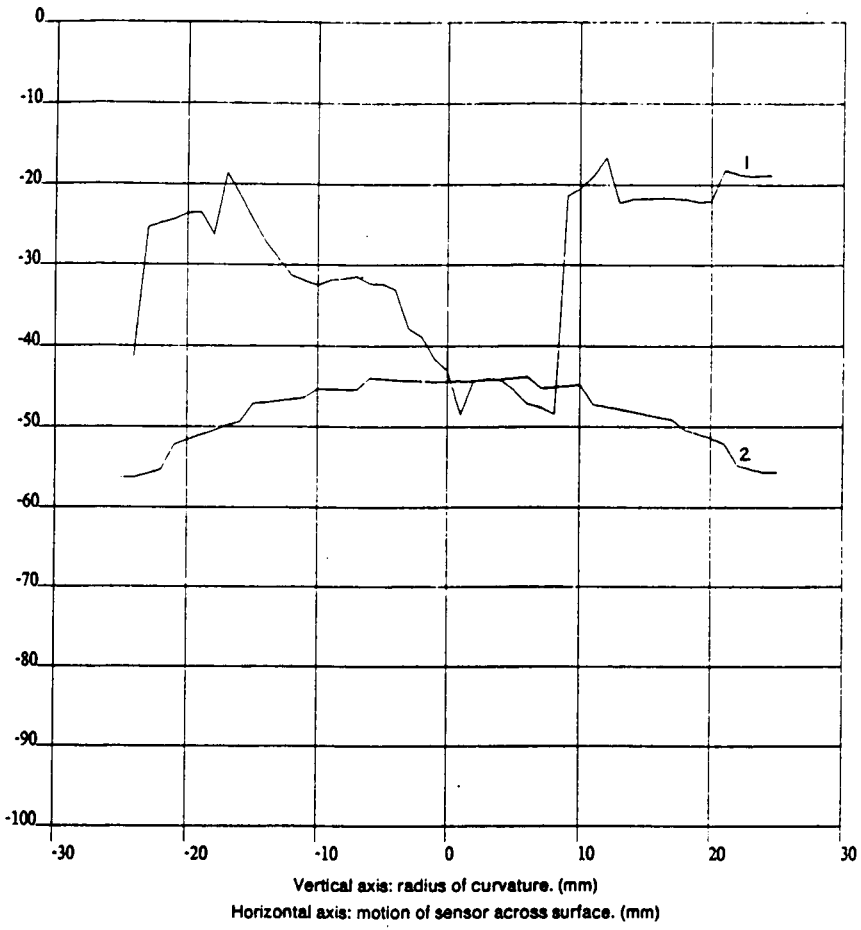

Figure 19: The smaller principal radius of curvature of a cone: measured 1 and simulated 2 results, and the actual value 3.

has a range of 10 cm where it can measure distance with a precision of 0.1 mm and surface orientation with a precision of 1.0°. The sensor can acquire data at a rate exceeding 200 points per second.

The design of the proximity sensor was guided by a statistical analysis of the uncertainty in the measurement of position using a single light source and the measurement of surface orientation using several light sources. The analysis related the number of light sources needed to measure orientation

within a specified accuracy to the distribution of light spots on a target surface. The new design is also intended to be a compact sensor for use on a robotic manipulator.

The proximity sensor is subject to error because of various types of distortion, nonlinearity, and noise. To compensate for the distortion of the sensor chip and imaging optics, a square array of light spots was generated in the field of view. A two dimensional transform was computed that maps the measured image of this array on the sensor chip into its ideal undistorted image. This transform was applied to the sensor chip coordinates during the operation of the sensor.

To further compensate for errors in the computation of distance, error correcting polynomials were computed that map the distance of a surface computed by triangulation into its actual distance. These polynomials were used during the operation of the sensor to improve measurement results.

The features of this proximity sensor include its simple principle of operation and its fast speed. The sensor chip which detects the spot of light on the target surface is an analog device which outputs the position of the centroid of a spot of light on its surface. Although the accuracy of any individual measurement of light spot position is limited by the distortion of a spot of light by a surface, and the noise and sensitivity of the sensor, we take advantage of the speed of the sensor and use multiple light sources to increase the overall accuracy of measurements. The geometrical arrangement of the light sources was guided by the statistical analysis to achieve the design specification for accuracy. Measurement of distance, surface orientation and surface curvature can exploit the geometrical redundancy of the device.

Acknowledgments

We thank Regis Hoffman and Donald Schmitz for useful discussions and help in software and hardware development. This research was partially supported by the Office of Naval Research (ONR) Grant No. N00014-81-K-0503, and by the National Science Foundation Grant No. ECS-8320364.

References

[1] Bamba, T.,Maruyama, H., Kodaira, N. and Tsuda, E.
A Visual Seam Tracking System for Arc Welding Robots.
In *Fourteenth International Symposium on Industrial Robots*, 1984.

[2] Bamba, T.,Maruyama, H., Ohno, E. and Shiga, Y.
A Visual Sensor for Arc Welding Robots.
In *Eleventh International Symposium on Industrial Robots*. 1982.

[3] Bejczy, A.
Smart Sensors for Smart Hands.
Nasa Report Number 78-1714, 1978.

[4] Bevington, Philip R.
Data Reduction and Analysis for the Physical Sciences.
McGraw-Hill Book Company, 1969.

[5] Diffracto Limited.
Diffracto Robotics Vision Sensors.

[6] Fuhrman, M. and Kanade, T.
Design of an Optical Proximity Sensor using Multiple Cones of Light for Measuring Surface Shape.
Technical Report TR-84-17, Carnegie Mellon University Robotics Institute, 1984.

[7] Hayes, J.G.
Numerical Aproximation to Functions and Data.
Athlone Press, University of London, 1970.

[8] Kanade, T. and Sommer, T.
An Optical Proximity Sensor for Measuring Surface Position and Orientation for Robot Manipulation.
Technical Report TR-83-15, Carnegie Mellon University Robotics Institute, 1983.

[9] Kanade, T. and Asada, H.
Noncontact visual three-dimensional ranging devices.
In B. R. Altschuler (editor), *3-D Machine Perception*, page 48-53. SPIE, 1981.

[10] Lipschutz, M. M.
Schaum's Outline of Theory and Problems of Differential Geometry.
McGraw Hill Book Co., 1969.

[10] Morander, E.
The Optocator. A High Precision, NonContacting System for Dimension and Surface Measurement and Control.
In *Proc. Fifth Intern. Conf. on Automated Inspection and Product Control*, pages 393-396. , 1980.

[12] Nakamura, Y., Hanafusa, H.
A New Optical Proximity Sensor for Three Dimensional Autonomous Trajectory Control of Robot Manipulators.
In *Proceedings: '83 International Conference on Advanced Robotics*. 1983.

[13] Okada, T.
A Short Rangefinding Sensor for Manipulators.
Bulletin of Electrotechnical Laboratory 42, 1978.

[14] Thring, M.W.
Robots and Telechirs.
Ellis Horwood Limited, 1983.